Tuning the Magnetic Properties and Structural Stabilities of the 2-17-3 Magnets Sm_{2}Fe_{17}X_{3} (X=C, N) by Substituting La or Ce for Sm

Tribhuwan Pandey, Mao-Hua Du, and David S. Parker

Tuning the magnetic properties and structural stabilities of the 2-17-3 magnets $Sm_2Fe_{17}X_3$ (X = C, N) by substituting La or Ce for Sm[*]

Tribhuwan Pandey,[†] Mao-Hua Du, and David S. Parker[‡]

Material Science and Technology Division, Oak Ridge National Laboratory Oak Ridge 37831 TN USA

Designing a permanent magnet with reduced critical rare earth content is of paramount importance in the development of cost effective modern technologies. Here, by performing comprehensive first-principles calculations we investigate the potential avenues for reducing the critical rare earth content in $Sm_2Fe_{17}N_3$ and $Sm_2Fe_{17}C_3$ by La/Ce substitution at Sm site. The calculated magnetic properties of base compounds are in good agreement with the previous low temperature (4.2 K) experimental measurements, and show a large axial anisotropy. Although La/Ce substitution results in slight reduction of magnetic anisotropy, the magnetic moments of Fe atoms mostly remain unchanged. In particular large axial anisotropies of 7.2, and 4.1 MJ/m^3 are obtained for $SmCeFe_{17}N_3$, and $SmLaFe_{17}N_3$, respectively. These values of anisotropies are comparable to the state of the art permanent magnet $Nd_2Fe_{14}B$. The foremost limitation of $Sm_2Fe_{17}X_3$ magnets for practical application is the formation nitrogen/carbon vacancies at high temperatures. By calculating the N(C) vacancy formation energy we show that La/Ce substitution enhances the vacancy formation energy. This will likely improve the thermodynamic stability of these alloys at high temperatures. Therefore, La/Ce-substituted $Sm_2Fe_{17}C_3$, and $Sm_2Fe_{17}N_3$ compounds are promising candidates for high-performance permanent magnets with substantially reduced rare earth content.

I. INTRODUCTION

Permanent magnets are essential for the development of the state of the art technologies such as super computers, electric cars, wind turbines as well as for energy conservation [1–6]. A good permanent magnet requires large value of magnetization, uniaxial anisotropy, large coercivity, high temperature stability, and high Curie temperature [5, 6]. In a permanent magnet, the local atomic moments are favorably aligned along a certain crystallographic direction, which can be characterized by the energy difference with the other spatial directions. This energy difference is often quantified as the magnetocrystalline anisotropy energy (MAE). The higher MAE usually results in high coercivity; making the demagnetization difficult. The anisotropy mainly arises from the coupling between spin and lattice also known as the spin orbit (L·S) coupling [7, 8]. Due to the localized nature of rare earth (RE) f-electrons, RE based alloys exhibits a large spin orbit coupling and as a consequence high values of MAE.

Materials based on RE and $3d$-transition metals (TM) form a large family of permanent magnets with excellent properties, such as $RE_2Fe_{14}B$, $RECo_5$, RE_2Co_{17}, and $RE_2Fe_{17}C_y$ compounds [9–15]. The notable example among these classes of RE compounds is $Nd_2Fe_{14}B$ [16–22]. The discovery of $Nd_2Fe_{14}B$ has also generated a lot of interest in RE_2Fe_{17} compounds. Although RE_2Fe_{17} class of compounds have large magnetization values, they suffer from low Curie temperatures and planar anisotropy constants. Over two decades ago Coey *et.al.* [23–25] reported that the nitrogenation/carbonation of Sm_2Fe_{17} and Y_2Fe_{17} *switches* magnetic anisotropy direction from planar to uniaxial and *enhances* their Curie temperature by *two* times. The microscopic origin of this strong ferromagnetism in $Sm_2Fe_{17}N_3$ and $Sm_2Fe_{17}C_3$ has been attributed to the lattice expansion and hybridization between nitrogen (carbon) and iron atoms [26, 27]. The RE-Fe-N compounds have been prepared with varying nitrogen stoichiometry [28, 29] and show high coercivities of $\sim$ 30 kOe [30]. These developments suggest that the $RE_2Fe_{17}N(C)_\delta$ compounds are attractive candidates for permanent magnets.

Although $RE_2Fe_{17}N(C)_\delta$ compounds exhibits promising magnetic properties, the resource criticality of RE elements such Nd, Dy, and Sm necessitates designing of permanent magnets without RE elements or less RE content [31]. In this regard, developing a permanent magnet with the use of abundant elements such as La and Ce instead of Sm/Nd [31] could be important for cost reduction. Another major problem with the technological application of $RE_2Fe_{17}N(C)_\delta$ compounds is their stability at high temperatures. $Sm_2Fe_{17}N_3$ ($Sm_2Fe_{17}C_3$) is meta-stable and decomposes to SmN (SmC) and α-Fe above 923 K temperature, making it difficult to fabricate sintered magnets [32, 33]. Therefore, improving the stability of Sm-Fe-N(C) magnets is another key issue.

In this work we explore the possibilities of reducing the critical RE content (Sm) in $Sm_2Fe_{17}N_3$ ($Sm_2Fe_{17}C_3$) by La and Ce substitution at Sm site. First, we explore the magnetic properties such as magnetic moments, exchange interactions as well as anisotropy constants for both pristine and La/Ce substituted systems. For the base compounds $Sm_2Fe_{17}N_3$ and $Sm_2Fe_{17}C_3$, in agreement with previous experimental studies, we find large axial anisotropies of 13.5 and 3.3 MJ/m^3, respectively. We observe that both $Sm_2Fe_{17}N_3$ and $Sm_2Fe_{17}C_3$ maintain axial anisotropies along with high

---

saturation magnetization even after La/Ce substitution. In particular axial anisotropies of 7.2, and 2.7 MJ/m^3 was found for SmCeFe$_{17}$N$_3$, and SmCeFe$_{17}$C$_3$, respectively. Next, we explore the effect of La/Ce substitution on the stability of Sm$_2$Fe$_{17}$N$_3$ (Sm$_2$Fe$_{17}$C$_3$), by calculating N(C) vacancy formation energy. The substitution of La/Ce in the lattice significantly improves the stability against nitrogen (carbon) vacancy formation, which will improve their stability at high temperatures. Our results indicate that the Sm content in Sm$_2$Fe$_{17}$X$_3$ (where X is either N or C) can be reduced by 50% with slight reduction in magnetic properties. These results chalk out the pathways for development of new magnetic materials with reduced RE content, which could be very effective in producing low cost permanent magnets.
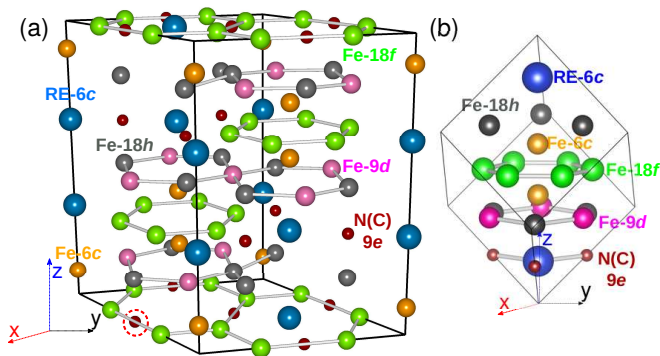

FIG. 1. (a) Crystal structure of the rhombohedral (Th$_2$Zn$_{17}$-type) allotropes of Sm$_2$Fe$_{17}$X$_3$ (a) 66 atom unit-cell (b) 22 atom primitive cell along with the crystallographic directions mapped according to the unitcell. All non equivalent crystallographic sites are also marked by the corresponding atom color. The circled red atom denotes the N/C atom removed for modeling a cell with N/C vacancy.

II. COMPUTATIONAL APPROACH

Calculations were performed using the all electron density functional theory code WIEN2K [34–36] together with the generalized gradient approximation of Perdew, Burke, and Ernzerhof [37]. The sphere radii were set to 2.50, 1.88, 1.61, and 1.61 Bohr for Sm, Fe, N, and C. For good convergence RK$_{max}$ (the product of the smallest sphere radius and the largest plane wave expansion wavevector) of 7.0 was used. All calculations were performed with the experimental lattice parameters [38–40] and all internal coordinates were relaxed until forces on all the atoms were less than 1 mRyd/Bohr. Experimental lattice parameters along with the GGA optimized lattice parameters are shown in Table V in the Appendix. The GGA optimized lattice parameters are in nice agreement with experiments. We also checked the dependence of optimized lattice parameters on Hubbard U. The lattice parameters were found to be very sensitive to the U value used, hence in order to model a reliable system all the computation presented in this work are done with the experimental lattice parameters. For La/Ce substitution at Sm site, one out

of two Sm atoms in the primitive cell was replace by La/Ce. These substituted structure were subsequently relaxed to their ground state by minimizing the forces on all the atoms. For the structure relaxation 1000 **k**-points were used in the full Brillouin zone. On going from Sm$_2$Fe$_{17}$N$_3$ (Sm$_2$Fe$_{17}$C$_3$) to Ce$_2$Fe$_{17}$N$_3$ (Ce$_2$Fe$_{17}$C$_3$) the cell volume varies nominally by 0.2% (0.4%), hence for the substituted compounds the lattice parameter was fixed at the corresponding values for parent nitrides and carbides.

All the calculations were performed by assuming a co-linear spin arrangement. The magnetic anisotropy energy (MAE) was obtained by calculating the total energies of the system with spin orbit coupling (SOC) as K = E$_a$ − E$_c$, where E$_a$ and E$_c$ are the total energies for the magnetization oriented along the a (11$\bar{2}$ in a rhombohedral primitive cell) and c (111 in a rhombohedral primitive cell) directions, respectively. Positive (negative) K corresponds to uniaxial (planar) anisotropy. Although the calculation of MAE from first-principles methods is somewhat difficult, as shown in some recent studies [22, 41–45] precise calculations often produce MAE in good agreement with experiments. To ensure the accuracy of MAE, its convergence with respect to number of **k**-point was carefully checked. The difference in MAE calculated using 2,000 and 3,000 **k**-points was less than 1.5% as shown in the Appendix Fig. 7(a). All the MAE values reported in this paper correspond to 2000 reducible **k**-points in the full Brillouin zone.

A number of different methodologies has been developed for accurate treatment of correlated nature of RE f-electrons. For example the self-interaction-corrected local spin density (SIC-LSD) scheme [46, 47], can provide insights into localized and band-like features of f-electrons. Alternately DFT+U approach introduces an effective Hubbard U parameter that separates the f-bands into lower and upper Hubbard bands. Here, the strong interactions between the Sm/Ce-f electrons were included by incorporating a Hubbard "U" correction. The U value for Sm site was obtained by optimizing the various magnetic properties (MAE, magnetic moments) with respect to the available experimental data. The obtained U values lie in the typical range that has been used before to correctly describe the magnetic properties of Sm based compounds [44, 48–50]. The convergence of MAE for Sm$_2$Fe$_{17}$N$_3$ and Sm$_2$Fe$_{17}$C$_3$ with respect to U parameter is shown in the Appendix Fig. 7(b). In order to optimize the U value for Ce substituted compounds (*i.e.* for SmCeFe$_{17}$N$_3$ and SmCeFe$_{17}$C$_3$) we calculated the MAE by varying U at the Ce site for a fixed U$_{Sm}$ value which is shown in the Appendix Fig. 8(a) and (b). On varying U$_{Ce}$ from 3 eV to 6 eV the MAE varies by < 10% for both the systems. All the calculation presented in this work are done with U$_{Sm}$ = 6.0 eV, and U$_{Ce}$ = 3.0 eV with the Hund′s coupling parameter J as zero. The addition of Hubbard U requires the double-counting correction terms in the energy functional to account for the fact that the Coulomb energy is already included in the DFT functional. To this end, here the self interaction correction scheme [51–53] (also known as fully localized limit (FLL) [44, 54] is used where onsite Coulomb interaction for localized orbitals is parametrized by U$_{effective}$ = U − J. It

is important to mention that due to presence of localized f-orbitals, DFT+U calculations for RE based compounds often may converge in a metastable state. Hence to find the actual ground state different starting configurations with varying f-orbital occupancies were used. After self consistent cycle the system always converged to a complex m states (pure atomic like m states were never reached). As our calculated magnetic moments and other properties are in reasonable agreement with experiments we assume that we have actual ground state.

For the nitrogen/carbon vacancy formation energy calculations a 66 atoms unitcell (UC) was used for both $Sm_2Fe_{17}N_3$ and $Sm_2Fe_{17}C_3$. This large unit-cell provides enough distance between the periodic images of nitrogen/carbon vacancies with in-plane distance being 8.74 Å and out-of-plane distance being 12.57 Å. The full structural relaxation of internal positions for pristine (defect free) unicells and unitcells with nitrogen/carbon vacancy were preformed until the residual forces were smaller than 2 mRyd/Bohr. The calculations were converged on a $4 \times 4 \times 4$ Γ centered **k**-point grid including spin polarization. For all the vacancy calculations the lattice parameters were fixed at the corresponding values for parent nitrides and carbides. These calculations were also performed using WIEN2K code. The Formation energy of N/C vacancy (ΔE_f) was defined as following:

$$\Delta E_f = E_{UC}^{N(C)vac} - E_{UC}^{Pristine} - E_{N(C)} \qquad (1)$$

Where, $E_{UC}^{N(C)vac}$ denotes energy of the unitcell with nitrogen/carbon vacancy, $E_{UC}^{Pristine}$ is the energy of the pristine unitcell, and last term is the total energy per atom for nitrogen/carbon. Here N_2 molecule and graphite were used as a reference to obtain the total energy for nitrogen and carbon atom. The formation energy values were also recalculated by including spin orbit coupling and Hubbard U.

III. RESULTS AND DISCUSSION

The RE_2TM_{17} allotropes exist in two different crystal structure; the rhombohedral Th_2Zn_{17}-type and the hexagonal Th_2Ni_{17}-type structure. The rhombohedral structure is stable for the light RE elements (from Ce to Eu), whereas for the heavy RE elements (from Gd to Lu) the hexagonal structure is most stable. As shown in Fig. 1 (a) and (b) the Th_2Zn_{17} structure is a layered structure built from close-packed Fe-layers alternated by mixed layers of RE-Fe. The elements with small atomic radii such as nitrogen, carbon, and hydrogen occupy the interstitial sites ($9e$) as shown in Fig. 1 (a), which in turns improves the magnetic properties of these compounds [38, 39].

To check the stable ground state, calculations were performed for three different magnetic configurations (i) RE atoms are aligned with respect to Fe atom (FM) (ii) RE atoms are anti-aligned with respect to Fe atoms (AFM), and (iii) non-magnetic (NM) configuration. The corresponding energies with respect to NM state are listed in Table I. For all three system Sm_2Fe_{17}, $Sm_2Fe_{17}N_3$, and $Sm_2Fe_{17}C_3$ we find the

TABLE I. The calculated relative energies per Fe atom for ferromagnetic (FM) and anti-ferromagnetic (AFM) arrangement of Fe atoms with respect to RE atoms. The presented energies are calculated with respect to non magnetic (NM) configuration on per Fe atom basis.

Compound	E_{NM} (meV)	E_{FM} (meV)	E_{AFM} (meV)	J_{RT} (meV)
Sm_2Fe_{17}	0	−684.3	−759.3	−1.9
$Sm_2Fe_{17}N_3$	0	−802.0	−850.0	−1.3
$Sm_2Fe_{17}C_3$	0	−746.0	−789.0	−1.3

ground state to have the Sm spin moment opposite to that of the Fe, with an energy cost relative to Fe-Sm NM alignment as 759.3, 850 and 789 meV per Fe atom. These energies can be used to compute the RE-Fe exchange couplings (J_{RT}) within the two-sublattice model. Within this model the J_{RT} is defined as [55, 56]

$$J_{RT} = \frac{E_{AFM} - E_{FM}}{4 S_{RE} S_{Fe} Z_{RE} Z_{Fe}} \qquad (2)$$

Here E_{AFM} and E_{FM} are the total energies of the ferromagnetic and anti-ferromagnetic configuration. S_{RE}, and S_{Fe} are the spin moment of RE, and Fe sublattice, respectively. For these calculations S_{Fe} is averaged over four crystallographically nonequivalent Fe sites. Z_{Fe} and Z_{RE} are the number of nearest neighboring Fe atoms around the RE atom and the number of RE elements in the simulation cell, respectively. The above expression leads to a Sm-Fe exchange coupling parameter (J_{RT}) of −1.9, −1.3, and −1.3 meV for Sm_2Fe_{17}, $Sm_2Fe_{17}N_3$, and $Sm_2Fe_{17}C_3$ as shown in Table I. For $Sm_2Fe_{17}C_3$, and $Sm_2Fe_{17}N_3$ we see a slight reduction in J_{RT} when compared to Sm_2Fe_{17}. Similar value of J_{RT} has been reported for $RE_2Fe_{14}B$ family of magnets [55, 57, 58].

The magnetic moments for Sm_2Fe_{17} and its nitride ($Sm_2Fe_{17}N_3$) and carbide ($Sm_2Fe_{17}C_3$) are shown in Fig. 2(a) and summarized in Table II. Our calculated magnetic moments and those obtained from other electronic structure calculations for parent compound Sm_2Fe_{17} and its nitride and carbide [27, 56, 59, 60] show good qualitative agreement. The quantitative comparison is a bit difficult as these calculations differ in the treatment of the $4f$ electrons [27, 56, 61], lattice parameters and atomic positions. The calculated Fe orbital moments for Sm_2Fe_{17} lies in between 0.04 to 0.05 μ_B, which are shown in Table II in the parentheses. The Fe orbital moments are enhanced when interstitial nitrogen/carbon is inserted, and the enhancement is higher for $Sm_2Fe_{17}C_3$. Furthermore, on introducing nitrogen/carbon interstitial atoms, while the spin moment of Fe-$18f$ and Fe-$18h$ sites, which are close to N/C atoms are slightly decreased, the moments on the more distant Fe-$9d$ site are enhanced as shown in Table II and Fig. 3 (a) and (b). This trend of Fe moments on nitrogenation/carbonation is in good qualitative agreement with previous studies and has been attributed to hybridization between N(C) and Fe atoms [26, 27]. Regardless of this slight variation the average Fe-spin moment of these systems remains in the range of 2.36-2.44 μ_B, which is significantly higher than the value for BCC Fe 2.2 μ_B. The Sm total magnetic mo-
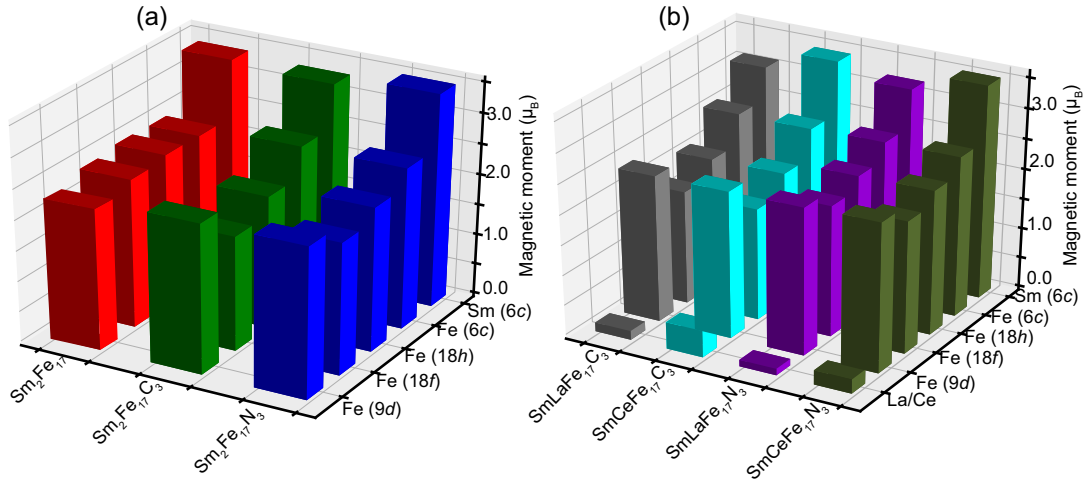
FIG. 2. The calculated total (orbital + spin) magnetic moments at various non equivalent atomic sites for (a) pristine and (b) La/Ce substituted systems. The calculated magnetic moments on rare earth (RE) atoms are negative and shown here as positive.
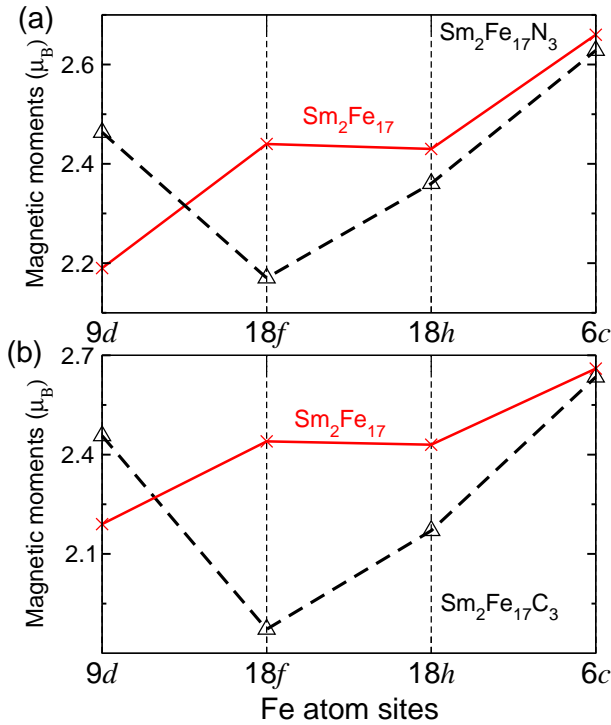

FIG. 3. The calculated total (spin + orbital) magnetic moments on Fe sites for (a) $Sm_2Fe_{17}N_3$, and (b) $Sm_2Fe_{17}C_3$. Total magnetic moments of various Fe-sites in Sm_2Fe_{17} are also shown for comparison. Total (spin + orbital) magnetic moments on various Fe-sites remain independent of U_{Sm} used and the main impact of U is only at MAE.

ments are also listed in Table II and displayed in Fig. 2(a). The variation in Sm orbital and spin magnetic moments for both $Sm_2Fe_{17}N_3$ and $Sm_2Fe_{17}C_3$ are shown in the Appendix Fig. 9. The calculated orbital moment of Sm atoms without U is rather small (1.58 μ_B for $Sm_2Fe_{17}N_3$ and 1.79 μ_B for

$Sm_2Fe_{17}C_3$. On varying U in GGA+SOC+U calculations the orbital moment of Sm atoms increases rapidly and saturates at higher values of U. The rate of increase of orbital moments with U is higher for nitrogen interstitial compound than in carbon interstitial compound. The variation of Sm spin moments with U parameter is also shown in the inset of Fig. 9. As expected the Sm spin moments display very weak dependence on U values. For $U_{Sm} = 6$ eV we see that, Sm atoms has large (~ 2.3 μ_B) orbital moment. For C interstitial compounds the orbital moment of Sm remains unchanged, however it slightly decreased in the case of N interstitial. The magnetic moment for La/Ce substituted compounds can be found in Fig. 2(b) and Table II. As can be seen for the substituted compounds the magnetic moment on Fe and Sm sites remain more or less unchanged. On the other hand the magnetic moment on the substituted RE atomic sites (La/Ce) is quenched as La has no f electrons and Ce has only one outermost f electron.

Total magnetization in the parent, interstitial, and La/Ce substituted compounds are summarized in Table II. For the Sm_2Fe_{17} and interstitial compounds the calculated total magnetic moment agrees well with the experimental measured value by neutron diffraction [69, 70] or magnetization measurements at low temperature [1, 63, 71, 72]. We obtained a saturation magnetic moment of 1.2 and 1.4 T for $Sm_2Fe_{17}C_3$ and $Sm_2Fe_{17}N_3$, respectively, which is in fair agreement with the experimentally measured 4.2 K value as compared in Table II. Considering the notable difficulties associated with modeling of RE elements with first-principles methods this agreement is quite reasonable. Another reason for the deviation between calculated and measured data could be the non stoichiometric effects. Due to the reduced (negative) magnetic moment at La/Ce sites we see an enhanced total magnetic moments for the substituted compounds when compared to the $Sm_2Fe_{17}C_3$ and $Sm_2Fe_{17}N_3$.

Next, we turn our attention to MAE constant K_1, which is shown in Fig. 4 and Table II. The MAE represents the energy required for changing the orientation of the magnetic mo-

TABLE II. Calculated total (orbital + spin) magnetic moments at various atom sites in μ_B, total magnetic moment of the system (m_{tot}) in μ_B per formula unit, saturation magnetization (M_S) in Tesla, and magneto-crystalline anisotropy constant (K_1) in MJ/m^3 for Sm$_2$Fe$_{17}$, Sm$_2$Fe$_{17}$X$_3$, SmLaFe$_{17}$X$_3$, and SmCeFe$_{17}$X$_3$. The corresponding orbital moments are shown in the parentheses. Here X represents carbon or nitrogen atoms. These values are calculated including spin orbital coupling (SOC) with magnetization along [001] (111 in rhombohedral coordinates) direction with U value of 6 and 3 eV at Sm and Ce sites, respectively. Comparison of calculated and experimental total magnetization (in μ_B per formula unit) and K_1 (in MJ/m^3) is also shown. The contribution of RE atoms to MAE was quantified by calculating MAE with applying spin orbit coupling only at RE atoms (K_1^{RE}). Nearly 75 % MAE originates from RE atoms.

atom site	RE-Fe	RE-Fe-N			RE-Fe-C		
	Sm$_2$Fe$_{17}$	Sm$_2$Fe$_{17}$N$_3$	SmLaFe$_{17}$N$_3$	SmCeFe$_{17}$N$_3$	Sm$_2$Fe$_{17}$C$_3$	SmLaFe$_{17}$C$_3$	SmCeFe$_{17}$C$_3$
X(9e)		−0.05	−0.04	−0.043	−0.15	−0.15	−0.15
Fe(9d)	2.19(0.047)	2.48(0.053)	2.45(0.038)	2.48(0.05)	2.46(0.054)	2.43(0.048)	2.44(0.047)
Fe(18f)	2.44(0.041)	2.17(0.043)	2.18(0.034)	2.20(0.04)	1.89(0.047)	1.88(0.041)	1.86(0.040)
Fe(18h)	2.43(0.047)	2.37(0.056)	2.38(0.053)	2.40(0.058)	2.18(0.059)	2.14(0.058)	2.16(0.060)
Fe(6c)	2.66(0.049)	2.65(0.060)	2.65(0.046)	2.66(0.05)	2.65(0.068)	2.62(0.058)	2.62(0.056)
RE(6c)	−3.40(2.33)	−3.53(2.27)	−3.24(2.25)	−3.54(2.24)	−3.33(2.35)	−3.13(2.32)	−3.46(2.36)
La/Ce			−0.11(0.005)	−0.24(0.66)		−0.15(0.002)	−0.45(0.52)
m_{tot}	34.0	33.0	36.2	35.9	29.5	32.6	31.9
m_{tot}^{exp}	35.9[a]	38.2[b]			34.5[c]		
M_S (T)	1.47	1.37	1.51	1.50	1.24	1.37	1.34
M_S^{exp} (T)	1.03-1.20[d]	1.54-1.57[e]			1.45[f]		
K_1	−8.9	13.5	4.1	7.2	3.4	1.2	1.7
K_1^{exp}	−8.1[g]	13.1[h]			6.9[h]		
$K_1^{RE[i]}$	−6.9	10.5	3.5	5.3	2.3	1.0	1.2

[a] Sm$_2$Fe$_{17}$ Ref.[62]
[b] Sm$_2$Fe$_{17}$N$_{2.7}$ Ref.[1]
[c] Sm$_2$Fe$_{17}$C$_{2.3}$ Ref.[63]
[d] Sm$_2$Fe$_{17}$ Ref. [23, 29]
[e] Sm$_2$Fe$_{17}$N$_3$ Ref. [64, 65]
[f] Sm$_2$Fe$_{17}$C$_3$ Ref. [65]
[g] Sm$_2$Fe$_{17}$ Ref.[66]
[h] Sm$_2$Fe$_{17}$C$_2$(Sm$_2$Fe$_{17}$N$_{2.6}$) Ref.[67]
[i] MAE calculated by incorporating spin orbit coupling only at Sm/Ce/La sites.
[j] For comparison the state of art permanent magnet Nd$_2$Fe$_{14}$B has K_1^{exp} = 4.9 MJ/m^3 and m_{tot}^{exp} = 37.7 μ_B/f.u. [21, 68].

ments under the application of magnetic field. MAE is an essential quantity for achieving high coercivity in a permanent magnet. The MAE calculated without U parameter does not agree with experiments. In fact as shown in Fig. 4, even the sign of MAE cannot be predicted correctly. This indicates that in these systems correlation on Sm/Ce atoms are very important, and therefore we apply a on-site U parameter at both Sm and Ce that tends to localize the f electrons. The effect of on site Hubbard U parameter on MAE is clear from GGA+U calculations, which are shown in Fig. 7(b). Both Sm$_2$Fe$_{17}$C$_3$ and Sm$_2$Fe$_{17}$N$_3$ exhibit quite different dependence on U parameter. While for Sm$_2$Fe$_{17}$N$_3$, MAE exhibits a strong dependence on U, the U dependence of MAE for Sm$_2$Fe$_{17}$/Sm$_2$Fe$_{17}$C$_3$ is rather weak. This indicates that for RE magnets electron correlations play a central role in producing large MAE (coercivity), and explains why often LDA/GGA calculations under-

estimate the MAE of RE magnets. We find the parent compound Sm$_2$Fe$_{17}$ to be planar with K_1 value as −8.9 MJ/m^3, whereas for the C and N interstitial compounds a large positive MAE is seen. The positive sign of K_1 means that, as observed experimentally, the material is easy-axis which is favorable for permanent magnet application. Also the magnitude of K_1 is significantly higher than 2 MJ/m^3 that is a key requirement for high performance permanent magnets [5, 6]. In particular large axial anisotropies of 3.3 and 13.5 MJ/m^3 are obtained for Sm$_2$Fe$_{17}$C$_3$ and Sm$_2$Fe$_{17}$N$_3$, respectively. The measured anisotropy values from previous experimentally studies are also listed in Table II. Overall there is fair agreement between calculated and measured values. The discrepancy between theory and experiments can be associated to the non-stoichiometry of N/C in the experimental samples.

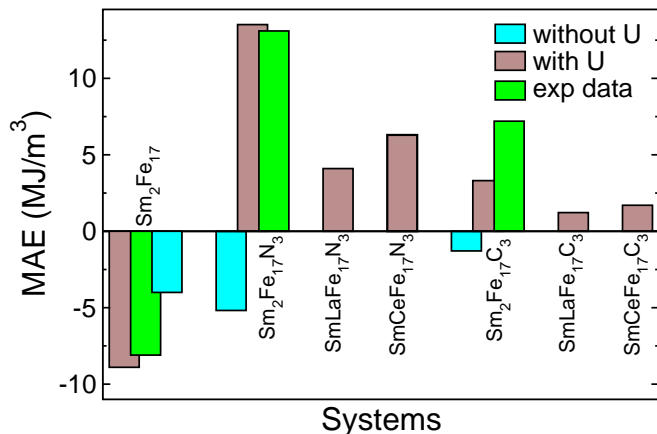The MAE in RE-TM magnets mainly originates from two

FIG. 4. The calculated magnetocrystalline anisotropy energy (MAE) for Sm_2Fe_{17}, $Sm_2Fe_{17}N_3$, $Sm_2Fe_{17}C_3$, and La/Ce substituted systems by including U parameters of 6 eV at Sm site and 3 eV at Ce site. The experimental MAE (filled green bars) and MAE obtained without U parameter (filled cyan bars) are also shown for comparison.

sources: (i) the MAE of Fe sub-lattice and (ii) single-site anisotropy of the Sm-f orbitals due to strong spin orbit coupling and crystal field effects [73–75]. In order to decouple the contribution to MAE from RE and Fe sub lattice, we ran the anisotropy calculation by switching off the spin orbit coupling at Fe sites, which is represented by K_1^{RE} in Table II. We see that contribution of RE atoms to MAE is more than 75%. This is in agreement with experiments where it is shown that the most of low temperature anisotriopy originates from RE sub lattice [1]. The experimental observation of switching of MAE from easy plane to easy axis for interstitial compounds is nicely reproduced by our calculations. As noted in Refs. [27, 75] this can be explained on the basis of crystal field. The second-order crystal field parameter (A_2^0) which determines the trend of MAE in RE magnets is significantly increased upon insertion of interstitial N or C, which helps is switching the direction of MAE from easy plane to easy axis. Similar mechanism has been proposed for explaining higher MAE of $SmCo_5$. As noted by Larson et.al [44, 74] for $SmCo_5$ and other related compounds, the comparable strength of crystal-field and spin-orbit effects, results in a large MAE in these compounds. At the same time the substantially weaker crystal-field effects results in a relatively smaller anisotropy in Sm_2Co_{17}.

We next evaluate effect of La/Ce contribution on MAE, which is shown in Fig. 4 and Table II. While for Ce substituted compounds the reduction in MAE is roughly proportional to the substituted Sm atoms, a higher reduction in MAE was observed for La substituted compounds. For example, in the case of $SmCeFe_{17}N_3$ and $SmLaFe_{17}N_3$ MAE is reduced by 40% and 70%, respectively. Although MAE is somewhat reduced after La/Ce substitution, it still maintains large positive values. Specifically, large axial anisotropies of 7.2, and 4.1 MJ/m^3 was obtained for $SmCeFe_{17}N_3$, and $SmLaFe_{17}N_3$, respectively, which are comparable to $Nd_2Fe_{14}B$ (4.9 MJ/m^3) [21, 68]. These results thus indicate that the La/Ce substituted sys-

tems could be promising for permanent magnet applications. Unlike $Sm_2Fe_{17}N_3$ and $Sm_2Fe_{17}C_3$, for Ce substituted compounds the experimental data of MAE is not available hence a *proper* U cannot be estimated by fitting the MAE to the experimental data. In order to optimized the U value for Ce substituted compounds (*i.e.* for $SmCeFe_{17}N_3$ and $SmCeFe_{17}C_3$) we calculate the MAE by varying U at the Ce site for a fixed U_{Sm} value which is shown in the Appendix Fig. 8 (a) and (b). On varying U_{Ce} from 3 eV to 6 eV the MAE varies only by $< 10\%$ for both the systems, and all the calculations reported here are done with U_{Ce} as 3 eV. Based on this analysis we conclude that our results are not very sensitive with respect to U_{Ce}.

The density of states (DOS) for crystallographically non-equivalent Fe-atoms in Sm_2Fe_{17}, and $Sm_2Fe_{17}N_3$ is shown in the Fig. 5 (a)-(d). Similar figure for $Sm_2Fe_{17}C_3$ is given in the Appendix Fig. 10. The DOS depicts behavior of a typical ferromagnetic system. The the partial density of states for RE atoms is compared in Fig. 6. We can see that the states near the Fermi level predominantly originate from of RE-f and Fe-d states. For Sm_2Fe_{17} there is an exchange splitting of $\sim$ 2-3 eV in the Fe-d states. The similar behavior is observed for $Sm_2Fe_{17}N_3$, and $Sm_2Fe_{17}C_3$. As shown in Fig. 5 (a-d) the spin-up Fe-d states are fully occupied in the base compound. On introducing interstitial nitrogen or carbon atoms, the d states of Fe-18h and Fe-18f atoms hybridize with the p states of interstitial atoms. As can be seen from Fig. 5 (a-d), in the vicinity of Fermi level, the Fe(18f) and Fe(18h) DOS for $Sm_2Fe_{17}N_3$ is relatively larger than in the base compound Sm_2Fe_{17}, which indicates the hybridization of these states with the interstitial nitrogen/carbon atoms. With N/C insertion, the majority spin states at the 18h and 18f Fe sites are broadened and the number of occupied spin-up electrons decreases. Furthermore the minority spin states shift towards lower-energy and the number of spin-down electrons increases resulting in a decrease in magnetic moments for these sites as shown in Fig. 3 (a) and (b). This observation is in agreement with the previous studies [27, 76]. Overall the Fe moments are larger than that in pure Fe, which contribute to the excellent magnetic properties of these compounds.

As shown in Fig. 6 (a), the RE-4f states are not occupied in the spin-up channel and are partially occupied in the spin-down channel, confirming that the Sm moments align in the opposite direction compared to the Fe moments. The Sm DOS for Sm_2Fe_{17} calculated within only GGA+SOC (without U) is also shown in Fig. 6 (a) by blue dotted lines. As can be seen, without U, the Sm-f orbitals form a narrow band which is pinned at the Fermi level (shown by blue dashed line). The addition of U shifts the unoccupied spin-up f band towards the high energy. Also the occupied spin-down bands splits into the lower and the upper Hubbard bands, separated roughly by 6 eV. The exchange splitting at the Sm-f states is similar to that of Fe-d orbitals, even though the f DOS is substantially narrower. The Sm-f orbital DOS for base and for nitrogen interstitial compound is compared in Fig. 6 (a). With N/C insertion, the f states shift to the lower-energy side. Since both the spin-up and spin-down states are pushed down to the lower energy, the change in the magnetic moment is not as large as
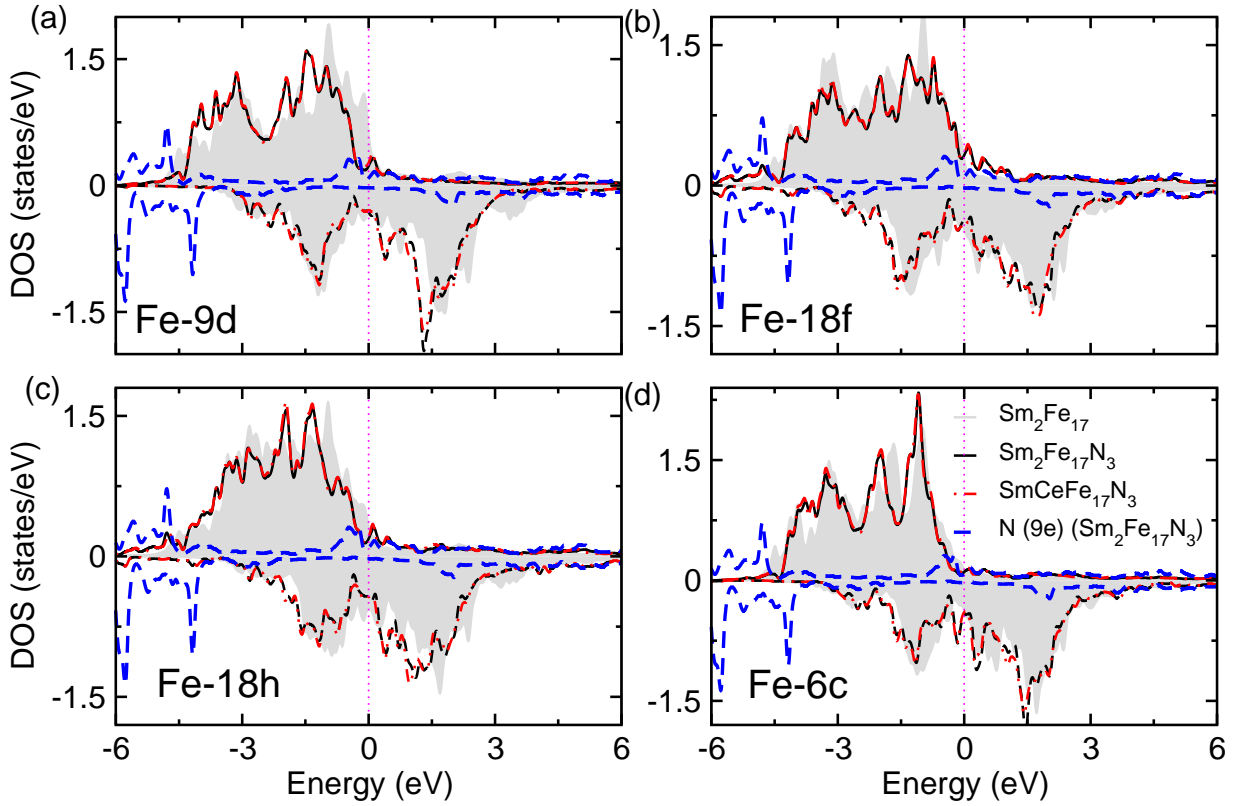
FIG. 5. The d orbital DOS of crystallographically non-equivalent Fe-atoms for Sm_2Fe_{17} (gray filled area), $Sm_2Fe_{17}N_3$ (black solid lines), and $SmCeFe_{17}N_3$ (red dashed lines). The panel (a)-(d) represents 9d, 18f, 18h, and 6c-Fe sites respectively. The p-orbital DOS for the 9e nitrogen interstitial atom in $Sm_2Fe_{17}N_3$ is also shown by blue dotted lines. The spin-up and spin-down states are shown in the upper and lower portions, respectively.

TABLE III. The calculated energy difference (ΔE) between the FM-state (where the spin moments on all the Fe atoms are aligned) and the AFM-state (where the spin moments on the neighbors of Fe atoms are anti-aligned) on per Fe atom basis. The calculated mean field Curie temperature $\left(\frac{1}{3}\Delta E\right)$ along with the experimental Curie point is also shown.

	Sm_2Fe_{17}	$Sm_2Fe_{17}N_3$	$SmLaFe_{17}N_3$	$SmCeFe_{17}N_3$	$Sm_2Fe_{17}C_3$	$SmLaFe_{17}C_3$	$SmCeFe_{17}C_3$
ΔE (meV)	-117.0	-264.7	-289.0	-306.7	-251.8	-256.5	-273.5
T_C (K)	453	1024	1117	1187	974	1024	992
T_C-Exp. (K)	390 [67]	749 [67]			680 [67]		

those at the Fe sites. The unoccupied f states are broadened by the insertion of N/C. The structure of the occupied f states remains more or less same for all the compounds.

To understand the effect of La/Ce substitution at the Sm sites on the magnetic properties of these compounds, we next analyze their electronic structure. The partial Fe d-DOS and Sm f-DOS for the substituted systems are presented in Fig. 5 (a-d), and Fig. 6 (b-c) respectively. The similar figures for carbon interstitial compounds is given in the Appendix Fig. 10 (a-d) and Fig. 11 (b-c). As can be seen the Sm/La substitution has no effect on Fe d-DOS, and Fe-DOS overlaps with the equivalent curve for $Sm_2Fe_{17}N_3$/$Sm_2Fe_{17}C_3$. This explains why the moments on Fe sites remains unchanged on

Ce/La substitution. The only significant change in the DOS is at the RE-f states, which are shifted to higher energies by ~ 0.1 eV. For La/Ce substituted compounds the peak of Sm DOS in the vicinity of Fermi level is reduced, the reduction being higher for La substitution. This reduction in RE DOS is responsible for the reduction in MAE, seen with La/Ce substitution. As the reduction in RE-DOS is more prominent for La substituted compounds, the MAE for the La substituted compounds shows larger reduction (60-70%) in comparison to Ce substituted compounds (40-45%). The decrease in MAE of $Sm_2Fe_{17}N_3$ on Ce substitution can also be explained by difference in the prolaticity of RE $4f$ electron clouds in Sm and Ce. As explained by Sellmyer $et.al$ [75] due to less number

of electrons the $4f$ electron clouds in Ce are in the shape of an oblate, whereas in Sm it takes a shape of a prolate. Replacing a prolate ion (Sm in this case) by an oblate ion tends to reduce the MAE.
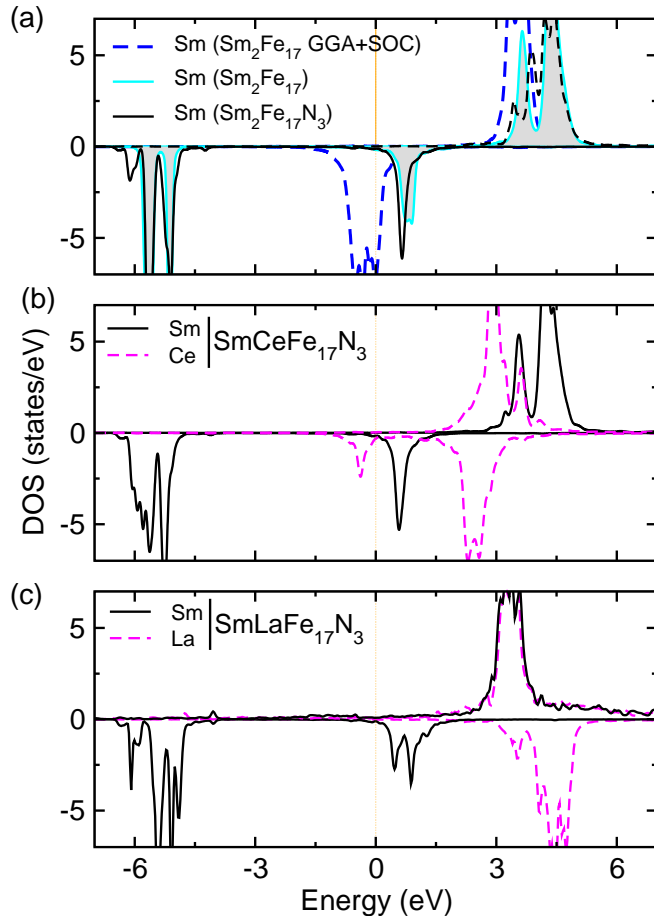

FIG. 6. The RE $4f$ states DOS calculated with U_{Sm} as 6 eV. (a) Comparison of Sm-$4f$ states in Sm_2Fe_{17} (gray filled) and $Sm_2Fe_{17}N_3$ (black solid lines). (b) The Sm (black solid lines) and Ce (magenta dashed lines) DOS in $SmCeFe_{17}N_3$. Here a U_{Ce} of 3 eV and U_{Sm} of 6 eV was used. (c) The Sm (black solid lines) and La (magenta dashed lines) DOS in $SmLaFe_{17}N_3$. The positive and negative portions represent spin-up and spin-down DOS, respectively. The Sm-f DOS from GGA+SOC (without U) calculation is also shown in (a) by blue dotted lines.

Next we estimate the effect of La/Ce substitution on Curie temperature (T_C). Within Heisenberg model the total energy of the system can be described as $E = \sum_{i,j} J_{ij} S_i \cdot S_j$. Here S_i and S_j are the atomic spins on sites i and j, respectively, and J_{ij} is the exchange energy between these spins. For estimating J_{ij} we calculated the energy difference between the ferromagnetic and antiferromagnetic structure (obtained by flipping the spin of most of the Fe-nearest neighbors). These configurations are shown in Fig. 12 in the Appendix. The resulting energy difference is listed in Table III. In mean-field approximation [77–79], the Curie temperature can be estimated as one third of this energy difference, measured on a per Fe basis. The base compounds Sm_2Fe_{17}, $Sm_2Fe_{17}C_3$,

and $Sm_2Fe_{17}N_3$ show a energy difference (ΔE) of -117.0, -251.8, and -264.7 meV, respectively between FM and AFM state. This in the mean-field approximation corresponds to a T_C of 453, 974, and 1024 K, respectively. Note that the mean field Curie point is over estimated compared to the available experimental values. Upon substituting La/Ce, the energy difference between FM and AFM-state increases by $\sim$ 5-9 % for $Sm_2Fe_{17}C_3$, and by 9-15% $Sm_2Fe_{17}N_3$. This suggests that the mean field exchange energy increases upon La/Ce substitution which in turn will increase the Curie temperature. It is worth mentioning that in the previous studies the increase in Curie temperature of base compound (Sm_2Fe_{17}) upon nitrogenation/carbonation has been attributed to enhanced Fe-Fe interaction due to the expansion of the unit cell. This is nicely reproduced by our calculations, where we see that ΔE for $Sm_2Fe_{17}C_3$/$Sm_2Fe_{17}N_3$ is more than two times larger than that for Sm_2Fe_{17}. We note that mean field approximation typically overestimates the transition temperature by around twenty percent or more, but is useful in determining an upper limit for T_C. The estimation T_C could be further improved by a atomistic spin dynamics simulations [80, 81] or within random phase approximation [82, 83].

As introduced before the main challenge with $Sm_2Fe_{17}N(C)_3$ compounds is their high temperature stability where they decomposed to SmN and Fe. In order to address the stability issue we calculated the formation energy (ΔE_f) of nitrogen(carbon) vacancy in the pure ($Sm_2Fe_{17}N_3$/$Sm_2Fe_{17}C_3$) and La/Ce substituted compounds. The results are shown in the Table IV. To check the reliability of our results formation energies were recalculated by including U for Sm and Ce atoms and with including spin orbit coupling. The ΔE_f show nominal changes in the formation energy upon inclusion of U and SOC as shown by ΔE_f(SOC+U) in Table IV. As can be seen, for La/Ce substituted systems we see that N/C vacancy formation energy increases by $\sim$ 20-50% (depending upon the system). As the vacancy formation energies may be sensitive to the choice of lattice parameters, it is important to check the reproducibility of the trend in formation energy with optimized lattice parameters. However doing it for all the system studied here is computationally expensive task. Also as mentioned before the experimental volume for Ce variants of 2-17-3 compounds (i.e $Ce_2Fe_{17}N_3$, and $Ce_2Fe_{17}C_3$) is only 0.5 % different than Sm counterparts [84] but no information is present for La version of these compounds. Here to test the reliability of our calculations we recalculated the nitrogen vacancy formation energy with DFT optimized lattices constants for $Sm_2Fe_{17}N_3$ and $SmLaFe_{17}N_3$. With the optimized lattice parameters for $Sm_2Fe_{17}N_3$, the nitrogen vacancy formation energy found to be 1.02 eV which is slightly lower than the value obtained with experimental lattice parameters. Similarly for $SmLaFe_{17}N_3$, a calculation with optimized lattice parameters gives nitrogen vacancy formation energy as 1.27 eV. We note that although with optimized lattice parameters the relative enhancement in the defect formation energy (25 %) is slightly reduced than the one obtained with experimental lattice parameters (36 %), it is still appreciably higher than the base compounds. This

TABLE IV. The calculated nitrogen/carbon vacancy formation energy (ΔE_f) for $Sm_2Fe_{17}X_3$, $SmLaFe_{17}X_3$, and $SmCeFe_{17}X_3$ (where X = N, and C). ΔE_f, and ΔE_f(SOC+U) denote that the formation energy calculated without and with SOC+U, respectively. As can be seen the La/Ce substitution enhances the N vacancy formation energy by more than $\sim 50\%$ and C formation energy by $\sim 60\%$.

ΔE_f	$Sm_2Fe_{17}N_3$	$SmLaFe_{17}N_3$	$SmCeFe_{17}N_3$	$Sm_2Fe_{17}C_3$	$SmLaFe_{17}C_3$	$SmCeFe_{17}C_3$
ΔE_f	1.18	1.60	1.85	0.53	0.77	0.90
ΔE_f(SOC+U)	1.20	1.64	1.81	0.52	0.79	0.88

indicates that La/Ce substitution may well stabilize these compounds against nitrogen(carbon) vacancy formation at high temperatures.

IV. CONCLUSIONS

In conclusion, we use first-principles calculations to understand the magnetic properties of Sm_2Fe_{17}, $Sm_2Fe_{17}C_3$, and $Sm_2Fe_{17}N_3$ compounds. We show that in the ground state of these compounds the magnetic moments of RE and Fe-atoms prefer to anti-align. The calculated magnetic properties of the base compounds agree well with available experimental data. In agreement with the experimental reports we find a large uniaxial anisotropies for $Sm_2Fe_{17}C_3$ and $Sm_2Fe_{17}N_3$. In order to to reduce the Sm content in these compounds, we further study the effect of La/Ce substitution at Sm site on magnetic properties. We show that although La/Ce substitution in these compounds tends to reduce the MAE, it still maintains large uniaxial values. The La/Ce substitution reduces the total moment on RE site. This works effectively in terms of improving the total magnetization since the magnetic moments of RE and Fe atoms anti-align with each other. As a consequence of La/Ce doping the exchange interaction energy increases, which in turn increases the Curie temperature. Furthermore, by calculating N/C vacancy formation energy we show that the La/Ce substitution will improve stability of these compounds at high temperatures against decomposition. Since all the La/Ce substituted compounds has 50% less Sm content and still maintains large axial anisotropy, high Curie point, large saturation magnetization, which makes them interesting for a permanent magnet with reduced critical rare earth content. We hope this investigation will be helpful for experimental processes of making high-performance $Sm_2Fe_{17}C_3$, and $Sm_2Fe_{17}N_3$ magnets with less Sm content.

APPENDIX
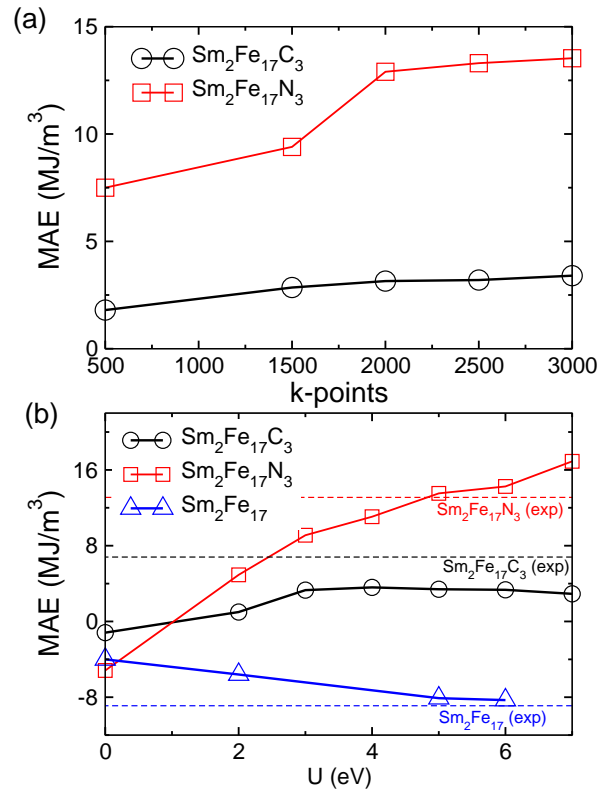
FIG. 7. (a) The dependence of MAE on the number of **k**-points used. The **k**-points convergence was checked at U = 6 eV. (b) The Hubbard U dependence of calculated magnetocrystalline anisotropy energy (MAE) for $Sm_2Fe_{17}N_3$, $Sm_2Fe_{17}C_3$, and Sm_2Fe_{17}. Experimental values are also marked for comparison with dashed lines. These calculations are performed by taking 2000 reducible **k**-points in Brillouin zone.
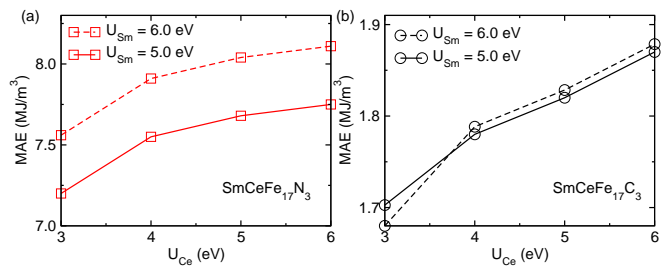
FIG. 8. The dependence of calculated MAE for $SmCeFe_{17}N_3$, and $SmCeFe_{17}C_3$ on Hubbard U parameter on Ce site at a fixed U_{Sm}. On varying U_{Ce} from 3 eV to 6 eV the MAE varies only by < 10%.

FIG. 9. U dependence of Sm orbital and spin (shown in the inset) magnetic moments for $Sm_2Fe_{17}N_3$, and $Sm_2Fe_{17}C_3$.

FIG. 10. The d orbital DOS of crystallographically non-equivalent Fe-atoms for for Sm_2Fe_{17} (gray filled area), $Sm_2Fe_{17}C_3$ (black solid lines), and $SmCeFe_{17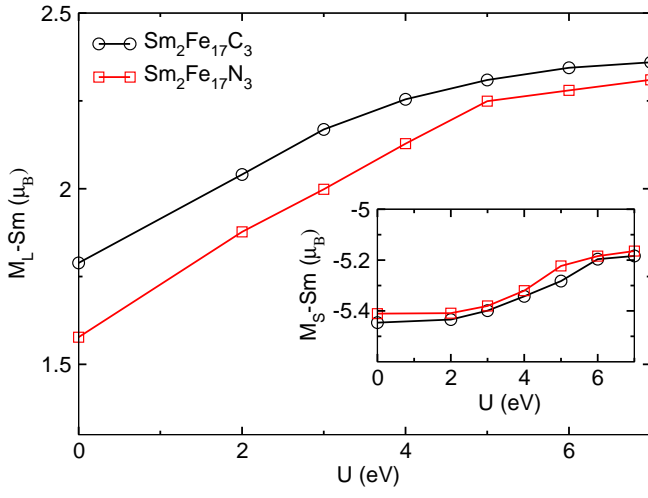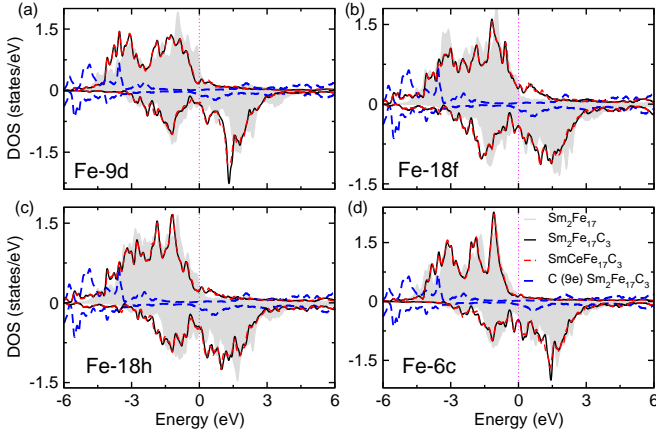}C_3$ (red dashed lines). The panel (a)-(d) represents 9d, 18f, 18h, and 6c-Fe sites respectively. The p-orbital DOS for the 9e carbon interstitial atom in $Sm_2Fe_{17}C_3$ is also shown by blue dotted lines. The spin-up and spin-down states are shown in the upper and lower portions, respectively. The Fe dos in $SmLaFe_{17}C_3$ exhibits similar features and not shown here.

TABLE V. The experimental a and c lattice parameters along with the DFT optimized lattice parameters (within GGA) for Sm_2Fe_{17}, $Sm_2Fe_{17}N_3$, and $Sm_2Fe_{17}C_3$. All the calculations reported in this work are performed with the experimental lattice parameters.

Compound	Exp		GGA	
	a (Å)	c (Å)	a (Å)	c (Å)
Sm_2Fe_{17}	8.558 [40]	12.441 [40]	8.55	12.46
$Sm_2Fe_{17}N_3$	8.743 [39]	12.659 [39]	8.70	12.68
$Sm_2Fe_{17}C_3$	8.744 [38]	12.572 [38]	8.70	12.53
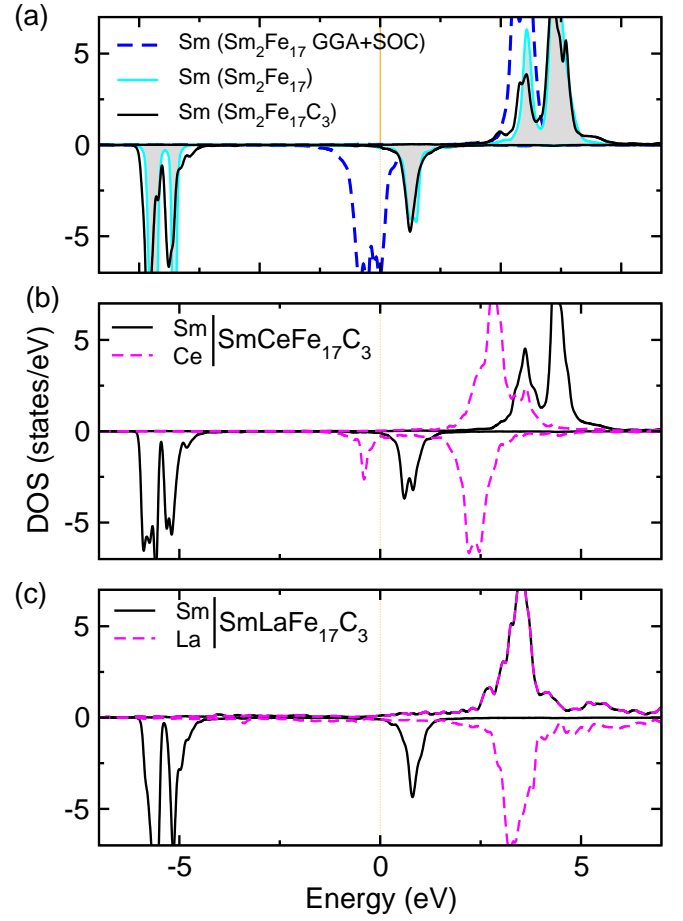
FIG. 11. The RE $4f$ states DOS calculated with U_{Sm} as 6 eV. (a) Comparison of Sm-$4f$ states in Sm_2Fe_{17} (gray filled) and $Sm_2Fe_{17}C_3$ (black solid lines). (b) The Sm (black solid lines) and Ce (magenta dashed lines) DOS in $SmCeFe_{17}C_3$. Here a U_{Ce} of 3 eV and U_{Sm} of 6 eV was used. (c) The Sm (black solid lines) and La (magenta dashed lines) DOS in $SmLaFe_17C_3$. The positive and negative portions represent spin-up and spin-down DOS, respectively. The Sm-f DOS from GGA+SOC (without U) calculation is also shown in (a) by blue dotted lines.
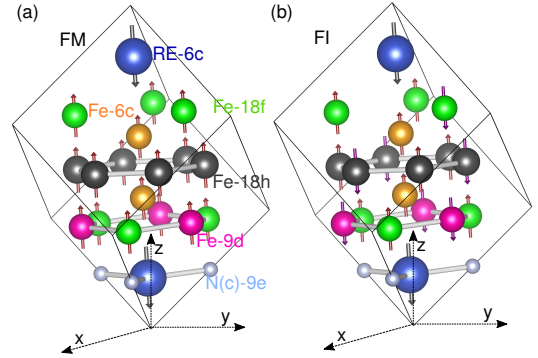
FIG. 12. Schematic defining the (a) Ferromagnetic (FM) and (b) Ferrimagnetic (FI) configurations of Fe atoms in the primitive cell used in Curie point calculations.

[1] K. Buschow, New developments in hard magnetic materials, Rep. Prog. Phys. **54**, 1123 (1991).

[2] K. H. J. Buschow, F. R. Boer, *et al.*, *Physics of magnetism and magnetic materials*, Vol. 92 (Springer, 2003).

[3] M. Kramer, R. McCallum, I. Anderson, and S. Constantinides, Prospects for non-rare earth permanent magnets for traction motors and generators, Jom **64**, 752 (2012).

[4] J. M. Coey, *Magnetism and magnetic materials* (Cambridge University Press, 2010).

[5] J. Coey, Hard magnetic materials: A perspective, IEEE Trans. Magn. **47**, 4671 (2011).

[6] J. Coey, Permanent magnets: Plugging the gap, Scr. Mater. **67**, 524 (2012).

[7] F. Bloch and G. Gentile, Zur anisotropie der magnetisierung ferromagnetischer einkristalle, Z. Phys. **70**, 395 (1931).

[8] H. Brooks, Ferromagnetic anisotropy and the itinerant electron model, Phys. Rev. **58**, 909 (1940).

[9] Z. Tie-Song, J. Han-Min, G. Guang-Hua, H. Xiu-Feng, and C. Hong, Magnetic properties of R ions in RCo_5 compounds (R= Pr, Nd, Sm, Gd, Tb, Dy, Ho, and Er), Phys. Rev. B **43**, 8593 (1991).

[10] W. Suski, N. Vityk, R. Gladyshevskii, A. Gilewski, T. Mydlarz, and K. Wochowski, Magnetic properties of $R_2Co_{17-x}Ga_x$ and $RCo_{5-x}Ga_x$ alloys (R = Y, Tb) in high magnetic fields, Chem. Met. Alloys **12**, 111 (2008).

[11] T. Shibata and T. Katayama, Magnetic properties of RCo_5 permanent magnets prepared by liquid phase sintering, Jpn. J. App. Phys. **12**, 1020 (1973).

[12] K. Konno, H. Ido, S. Cheng, S. Sankar, and W. Wallace, Al-substitution effects on the magnetic properties of RCo_5 (R= Y, Pr, Nd, and Sm), J. App. Phys. **73**, 5929 (1993).

[13] H. Tang, B. Shen, K. Buschow, F. De Boer, Y. Wang, and G. Qiao, Magnetic properties and structure of $R_2Co_{17-x}Ti_x$ intermetallic compounds (R = Pr or Nd), J. App. Phys. **81**, 5127 (1997).

[14] H. Xiu-Feng, J. Han-Min, W. Zi-Jun, T. Zhao, and C. Sun, Analysis of the magnetic properties of R_2Co_{17} (R= Pr, Nd, Sm, Gd, Tb, Dy, Ho, and Er), Phys. Rev. B **47**, 3248 (1993).

[15] D. Zhang, D. Middleton, E. Brück, F. De Boer, Z. Zhang, and K. Buschow, Magnetic properties of $R_2Co_{17-x}Ga_x$ compounds (R = Sm and Gd), J. Alloys Compd. **259**, 65 (1997).

[16] D. Givord, H. Li, and J. Moreau, Magnetic properties and crystal structure of $Nd_2Fe_{14}B$, Solid State Commun. **50**, 497 (1984).

[17] J. Holc, S. Beseničar, and D. Kolar, A study of $Nd_2Fe_{14}B$ and a neodymium-rich phase in sintered NdFeB magnets, J. Mater. Sci. **25**, 215 (1990).

[18] J. Coey, Intrinsic magnetic properties of compounds with the $Nd_2Fe_{14}B$ structure, J. Less Common Met. **126**, 21 (1986).

[19] J. Coey, Comparison of the intrinsic magnetic properties of $R_2Fe_{14}B$ and $R(Fe_{11}Ti)$; R= rare earth, J. Magn. Magn. Mater. **80**, 9 (1989).

[20] W. Rodewald and W. Fernengel, Properties of sintered Nd-Fe-TM-B magnets, IEEE Trans. Magn. **24**, 1638 (1988).

[21] J. Herbst, $R_2Fe_{14}B$ materials: Intrinsic properties and technological aspects, Rev. Mod. Phys. **63**, 819 (1991).

[22] M. A. Susner, B. S. Conner, B. I. Saparov, M. A. McGuire, E. J. Crumlin, G. M. Veith, H. Cao, K. V. Shanavas, D. S. Parker, B. C. Chakoumakos, *et al.*, Flux growth and characterization of Ce-substituted $Nd_2Fe_{14}B$ single crystals, J. Magn. Magn. Mater. **434**, 1 (2017).

[23] J. Coey and H. Sun, Improved magnetic properties by treatment of iron-based rare earth intermetallic compounds in anmonia, J. Magn. Magn. Mater. **87**, L251 (1990).

[24] H. Sun, Y. Otani, and J. Coey, Gas-phase carbonation of R_2Fe_{17}, J. Magn. Magn. Mater. **104**, 1439 (1992).

[25] H. Sun, J. Coey, Y. Otani, and D. Hurley, Magnetic properties of a new series of rare-earth iron nitrides: $R_2Fe_{17}N_y$ (y approximately 2.6), J. Phys. Condens. Matter **2**, 6465 (1990).

[26] H. Akai, M. Takeda, M. Takahashi, and J. Kanamori, Roles of light interstitials in magnetism of Fe, Solid state Commun. **94**, 509 (1995).

[27] L. Steinbeck, M. Richter, U. Nitzsche, and H. Eschrig, Ab initio calculation of electronic structure, crystal field, and intrinsic magnetic properties of Sm_2Fe_{17}, $Sm_2Fe_{17}N_3$, $Sm_2Fe_{17}C_3$, and Sm_2Co_{17}, Phys. Rev. B **53**, 7111 (1996).

[28] Y. Lu, O. Tegus, Q. Li, N. Tang, M. Yu, R. Zhao, J. Kuang, F. Yang, G. Zhou, X. Li, *et al.*, Magnetic anisotropy of (Sm, Y)$_2$Fe$_{17}$N$_y$ compounds, Physica B: Condensed Matter **177**, 243 (1992).

[29] M. Katter, J. Wecker, L. Schultz, and R. Grössinger, Magnetocrystalline anisotropy of $Sm_2Fe_{17}N_2$, J. Magn. Magn. Mater. **92**, L14 (1990).

[30] K. Schnitzke, L. Schultz, J. Wecker, and M. Katter, High coercivity in $Sm_2Fe_{17}N_x$ magnets, App. Phys. Lett. **57**, 2853 (1990).

[31] G. B. Haxel, J. B. Hedrick, G. J. Orris, P. H. Stauffer, and J. W. Hendley II, *Rare earth elements: critical resources for high technology*, Tech. Rep. (2002).

[32] X. Kou, R. Grössinger, M. Katter, J. Wecker, L. Schultz, T. Jacobs, and K. Buschow, Intrinsic magnetic properties of $R_2Fe_{17}C_yN_x$ compounds:(R= Y, Sm, Er, and Tm), J. Appl. Phys. **70**, 2272 (1991).

[33] X. Kou, R. Grössinger, X. Li, J. Liu, F. De Boer, M. Katter, J. Wecker, L. Schultz, T. Jacobs, and K. Buschow, Magnetic phase transition and magnetocrystalline anisotropy of $Sm_2Fe_{17}C_xN_y$, J. App. Phys. **70**, 6015 (1991).

[34] P. Blaha, K. Schwarz, G. K. H. Madsen, D. Kvasnicka, and J. Luitz, *WIEN2K, An Augmented Plane Wave + Local Orbitals Program for Calculating Crystal Properties* (Karlheinz Schwarz, Techn. Universität Wien, Austria, 2001).

[35] E. Sjostedt, L. Nordstrom, and D. J. Singh, An alternative way of linearizing the augmented plane-wave method, Solid State Commun. **114**, 15 (2000).

[36] D. J. Singh and L. Nordstrom, *Planewaves Pseudopotentials and the LAPW Method, 2nd ed.* (Springer, Berlin, 2006).

[37] J. P. Perdew, K. Burke, and M. Ernzerhof, Generalized gradient approximation made simple [phys. rev. lett. 77, 3865 (1996)],Phys. Rev. Lett. **78**, 1396 (1997).

[38] C. N. Christodoulou and T. Takeshita, Interstitial carbonation of the Sm_2Fe_{17} phase by reaction with hydrocarbons, J. Alloys Compd. **190**, 41 (1992).

[39] M. Katter, J. Wecker, C. Kuhrt, L. Schultz, and R. Grössinger, Structural and intrinsic magnetic properties of $Sm_2(Fe_{1-x}Co_x)_{17}N_y$, J. Magn. Magn. Mater. **114**, 35 (1992).

[40] C. Djega-Mariadassou, L. Bessais, A. Nandra, J. Grenèche, and E. Burzo, Structure and hyperfine properties of $Sm_2(Fe, Si)_{17}$, Phys. Rev. B **65**, 014419 (2001).

[41] B. C. Sales, B. Saparov, M. A. McGuire, D. J. Singh, and D. S. Parker, Ferromagnetism of Fe_3Sn and alloys, Sci. Rep. **4** (2014).

[42] D. S. Parker, N. Ghimire, J. Singleton, J. Thompson, E. D. Bauer, R. Baumbach, D. Mandrus, L. Li, and D. J. Singh, Magnetocrystalline anisotropy in UMn_2Ge_2 and related Mn-based actinide ferromagnets, Phys. Rev. B **91**, 174401 (2015).

[43] T. N. Lamichhane, V. Taufour, M. W. Masters, D. S. Parker, U. S. Kaluarachchi, S. Thimmaiah, S. L. Bud'ko, and P. C. Canfield, Discovery of ferromagnetism with large magnetic anisotropy in ZrMnP and HfMnP, Appl. Phys. Lett. **109**, 092402 (2016).

[44] P. Larson, I. Mazin, and D. Papaconstantopoulos, Calculation of magnetic anisotropy energy in $SmCo_5$, Phys. Rev. B **67**, 214405 (2003).

[45] J.-X. Zhu, M. Janoschek, R. Rosenberg, F. Ronning, J. Thompson, M. A. Torrez, E. D. Bauer, and C. D. Batista, LDA+DMFT approach to magnetocrystalline anisotropy of strong magnets, Phys. Rev. X **4**, 021027 (2014).

[46] J. P. Perdew and A. Zunger, Self-interaction correction to density-functional approximations for many-electron systems, Phys. Rev. B **23**, 5048 (1981).

[47] L. Petit, R. Tyer, Z. Szotek, W. Temmerman, and A. Svane, Rare earth monopnictides and monochalcogenides from first principles: towards an electronic phase diagram of strongly correlated materials, New J. Phys. **12**, 113041 (2010).

[48] X.-W. Yan, Y. Wang, M. Gao, D. Ma, and Z. Huang, Magnetic and electronic properties of samarium-doped phenanthrene from first-principles study, J. Phys. Chem. C **120**, 22565 (2016).

[49] C. Morari, F. Beiuşeanu, I. Di Marco, L. Peters, E. Burzo, S. Mican, and L. Chioncel, Magnetism and electronic structure calculation of SmN, J. Phys. Condens. Matter **27**, 115503 (2015).

[50] F. Aryasetiawan, K. Karlsson, O. Jepsen, and U. Schönberger, Calculations of Hubbard U from first-principles, Phys. Rev. B **74**, 125106 (2006).

[51] V. I. Anisimov, I. Solovyev, M. Korotin, M. Czyżyk, and G. Sawatzky, Density-functional theory and NiO photoemission spectra, Phys. Rev. B **48**, 16929 (1993).

[52] A. Liechtenstein, V. Anisimov, and J. Zaanen, Density-functional theory and strong interactions: Orbital ordering in Mott-Hubbard insulators, Phys. Rev. B **52**, R5467 (1995).

[53] I. Solovyev, P. Dederichs, and V. Anisimov, Corrected atomic limit in the local-density approximation and the electronic structure of d impurities in Rb, Phys. Rev. B **50**, 16861 (1994).

[54] E. R. Ylvisaker, W. E. Pickett, and K. Koepernik, Anisotropy and magnetism in the LSDA+U method, Phys. Rev. B **79**, 035103 (2009).

[55] M. Fähnle, K. Hummler, M. Liebs, and T. Beuerle, Ab initio electron theory for hard-magnetic rare-earth-transition-metal intermetallics, Appl. Phys. A. Mater. Sci. Process. **57**, 67 (1993).

[56] N. Drebov, A. Martinez-Limia, L. Kunz, A. Gola, T. Shigematsu, T. Eckl, P. Gumbsch, and C. Elsässer, Ab initio screening methodology applied to the search for new permanent magnetic materials, New J. Phys. **15**, 125023 (2013).

[57] E. Belorizky, M. Fremy, J. Gavigan, D. Givord, and H.-S. Li, Evidence in rare-earth (R)-transition metal (M) intermetallics for a systematic dependence of R-M exchange interactions on the nature of the R atom, J. Appl. Phys. **61**, 3971 (1987).

[58] J. Franse and R. Radwański, Magnetic properties of binary rare-earth 3d-transition-metal intermetallic compounds, Handbook of Magnetic Materials **7**, 307 (1993).

[59] W. Körner, G. Krugel, and C. Elsässer, Theoretical screening of intermetallic $ThMn_{12}$-type phases for new hard-magnetic compounds with low rare earth content, Sci. Rep. **6** (2016).

[60] S. Jaswal, W. Yelon, G. C. Hadjipanayis, Y. Wang, and D. J. Sellmyer, Electronic and magnetic structures of the rare-earth compounds $R_2Fe_{17}N_\xi$, Phys. Rev. Lett. **67**, 644 (1991).

[61] In the previous DFT studies on $Sm_2Fe_{17}N_3$ and $Sm_2Fe_{17}C_3$ the f electrons were treated in the "open core" approximation. This approxaimation does not allow direct hybridization of f-electron states with other valence-electron states. While the number of electrons in the $4f$ core to the one of a free RE^{3+} ion are fixed by charge density constraint, the spin density constraint fixes the magnetic spin moment of the $4f$ core to the value obtained from the R-S coupling.

[62] D. McNeely and H. Oesterreicher, Structural and low-temperature magnetic studies on compounds Sm_2Fe_{17} with aluminium substitution for iron, J. Less Common Met. **44**, 183 (1976).

[63] J. Coey and D. Hurley, New interstitial rare-earth iron intermetallics produced by gas phase reaction, J. Magn. Magn. Mater. **104**, 1098 (1992).

[64] T. Iriyama, K. Kobayashi, N. Imaoka, T. Fukuda, H. Kato, and Y. Nakagawa, Effect of nitrogen content on magnetic properties of $Sm_2Fe_{17}N_x (0< x< 6)$, IEEE Trans. Magn. **28**, 2326 (1992).

[65] O. Gutfleisch, Controlling the properties of high energy density permanent magnetic materials by different processing routes, J. Phys. D: Appl. Phys. **33**, R157 (2000).

[66] S. Brennan, R. Skomski, O. Cugat, and J. Coey, Anisotropy of easy-plane Y_2Fe_{17}, $Y_2Fe_{17}N_3$ and Sm_2Fe_{17}, J. Magn. Magn. Mater. **140**, 971 (1995).

[67] S. T. Oyama, in *The chemistry of transition metal carbides and nitrides* (Springer, 1996) pp. 1–27.

[68] Y. Otani, H. Miyajima, and S. Chikazumi, Magnetocrystalline anisotropy in Nd-Fe-B magnet, J. Appl. Phys. **61**, 3436 (1987).

[69] S. Miraglia, J. Soubeyroux, C. Kolbeck, O. Isnard, D. Fruchart, and M. Guillot, Structural and magnetic properties of ternary nitrides $R_2Fe_{17}N_x$ (R≡ Nd, Sm), J. Less Common Met. **171**, 51 (1991).

[70] O. Isnard, S. Miraglia, J. Soubeyroux, D. Fruchart, and J. Pannetier, Neutron powder-diffraction study of Pr_2Fe_{17} and $Pr_2Fe_{17}N_{2.9}$, Phys. Rev. B **45**, 2920 (1992).

[71] M. Katter, J. Wecker, C. Kuhrt, L. Schultz, and R. Grössinger, Magnetic properties and thermal stability of $Sm_2Fe_{17}N_x$ with intermediate nitrogen concentrations, J. Magn. Magn. Mater. **117**, 419 (1992).

[72] X.-P. Zhong, R. Radwański, F. De Boer, T. Jacobs, and K. Buschow, Magnetic and crystallographic characteristics of rare-earth ternary carbides derived from R_2Fe_{17} compounds, J. Magn. Magn. Mater. **86**, 333 (1990).

[73] S. Buck and M. Fähnle, Rare-earth magnetic anisotropy: Is the crystal field theory valid? J. Magn. Magn. Mater. **166**, 297 (1997).

[74] P. Larson and I. Mazin, Effect of lattice relaxation on magnetic anisotropy: Zr-doped Sm_2Co_{17}, Phys. Rev. B **69**, 012404 (2004).

[75] R. Skomski and D. Sellmyer, Anisotropy of rare-earth magnets, J.Rare Earths **27**, 675 (2009).

[76] M. Ogura, A. Mashiyama, and H. Akai, Role of N in the Permanent Magnet Material $Sm_2Fe_{17}N_x$, J. Phys. Soc. Jpn. **84**, 084702 (2015).

[77] N. Ashcroft and N. Mermin, *Solid State Physics* (Saunders College, Philadelphia, 1976).

[78] W. Nolting and A. Ramakanth, *Quantum theory of magnetism* (Springer Science & Business Media, 2009).

[79] P. W. Anderson, Theory of magnetic exchange interactions: exchange in insulators and semiconductors, Solid state physics **14**, 99 (1963).

[80] B. Skubic, J. Hellsvik, L. Nordström, and O. Eriksson, A method for atomistic spin dynamics simulations: implementation and examples, J. Phys. Condens. Matter **20**, 315203 (2008).

[81] R. F. Evans, W. J. Fan, P. Chureemart, T. A. Ostler, M. O. Ellis, and R. W. Chantrell, Atomistic spin model simulations of magnetic nanomaterials, J. Phys. Condens. Matter **26**, 103202 (2014).

[82] L. Sandratskii and P. Bruno, Exchange interactions and curie temperature in (Ga, Mn) As, Phys. Rev. B **66**, 134435 (2002).

[83] E. Şaşıoğlu, L. Sandratskii, P. Bruno, and I. Galanakis, Exchange interactions and temperature dependence of magnetization in half-metallic heusler alloys, Phys. Rev. B **72**, 184415 (2005).

[84] According to ICSD the unitcell volume for $Ce_2Fe_{17}N_3$ and $Ce_2Fe_{17}C_3$ is 839.70 $Å^3$ and 828.98 $Å^3$ which are quite close to the volume for $Sm_2Fe_{17}N_3$ (838.01 $Å^3$) and $Sm_2Fe_{17}C_3$ (832.44 $Å^3$).